Optimizing the synthesis of monodisperse colloidal spheres using holographic particle characterization

Christine Middleton, Mark D. Hannel, Andrew D. Hollingsworth, David J. Pine, and David G. Grier*

Department of Physics and Center for Soft Matter Research, New York University, New York, NY 10003

E-mail: david.grier@nyu.edu

Abstract

Holographic particle characterization measures the sizes and compositions of individual colloidal particles dispersed in fluid media and rapidly amasses statistics on the distributions of these properties, even for complex heterogeneous dispersions. This information is useful for analyzing and optimizing synthetic protocols. We illustrate how holographic characterization can guide process design through a case study on a particularly versatile model system composed of micrometer-scale spheres, which are synthesized from the organosilane monomer 3-(trimethoxysilyl)propyl methacrylate (TPM) and dispersed in aqueous media.

Introduction

Since the serendipitous discovery that emulsion polymerization can produce colloidal dispersions with very small polydispersity in size,[1,2] techniques for synthesizing monodisperse

colloidal particles have progressed through trial-and-error experimentation inspired by principles of chemistry and physics and validated ~~through~~ by batteries of particle-characterization measurements.[3–8] How process choices influence the properties of synthetic colloids typically can be gauged only after synthesis is complete; assessing the outcome ~~typically~~ often requires multiple orthogonal measurement techniques. Scanning electron microscopy, for example, is used to measure solid particles' size distribution and surface texture.[9] Mercury porosimetry and gas adsorption gauge their porosity[10] and surface area.[11] Refractometry and light scattering probe their optical properties.[12] Using such techniques to amass a representative set of characterization results takes time and requires expertise. Preparing samples for measurement, moreover, often involves transferring particles out of their native medium, and so can change their properties. Correlations among particles' properties are especially difficult to measure, particularly in heterogeneous dispersions.

Holographic particle characterization can streamline the design and optimization of colloidal synthesis processes by providing particle-resolved assays of samples' size distributions and compositions rapidly and with minimal sample preparation. Holographic characterization works equally well for droplets and solid particles. It naturally accommodates heterogeneous samples and reveals correlations between size and composition. Extensions to the technique provide particle-resolved morphology measurements from the same underlying data. All of this information about a sample's properties can be acquired with a single measurement in about ten minutes, which expedites systematic assays and can be fast enough to provide feedback for process control.

To illustrate the use of holographic particle characterization to guide process design, this work explores the roles of emulsion stoichiometry, initiator choice, and agitation conditions in the synthesis of monodisperse spheres of 3-(trimethoxysilyl)propyl methacrylate (TPM),[13] a model system with increasingly widespread applications in soft-matter research.[14–16] We apply holographic characterization to identify factors that influence size selection, polydispersity and composition and validate the results with conventional particle characteriza-

tion techniques. This study therefore builds on the work of van der Wel, *et al.*,[13] which ~~relies on~~ uses conventional techniques to systematically characterize the emulsion polymerization protocol for TPM spheres. Our holographic measurements independently confirm the observation [13] that smaller particles form at higher pH. They also reveal that more vigorous mixing yields larger particles without necessarily increasing polydispersity, a surprising trend that runs counter to common emulsion polymerization processes.

Materials and methods

Materials

The TPM monomer (3-(trimethoxysilyl)propyl methacrylate, 98 %) used in particle synthesis was purchased from Sigma Aldrich. Ammonium hydroxide (29 %) in water was added to adjust the pH of the synthesis environment. Two water-insoluble initiators, 2,2'-azobis(2-methylpropionitrile) (AIBN) and 1,1'-azobis(cyclohexanecarbonitrile) (ACHN) were purchased from Sigma Aldrich. Two water-soluble initiators, ammonium persulfate (APS) and potassium persulfate (KPS), also were purchased from Sigma Aldrich.

Emulsion polymerization

The protocols analyzed in this work focus on the influence of stir rate, pH, emulsion stoichiometry, and choice of radical initiation on the size, polydispersity, and refractive index of synthesized particles. While this list is not exhaustive, it illustrates choices made in optimizing synthetic protocols and the role that holographic characterization can play in making successful choices.

The synthesis begins with the formation of an emulsion of monodisperse TPM droplets. Monomeric TPM is insoluble in water but hydrolyzes into soluble monomers in the basic

environment of an aqueous ammonium hydroxide solution (pH > 9):

$$\mathrm{R{-}Si\,(OCH_3)_3 + 3\,H_2O \underset{\mathrm{pH>9}}{\overset{\mathrm{cat.}}{\rightleftharpoons}} R{-}Si\,(OH)_3 + 3\,CH_3OH,} \tag{1}$$

where

$$\mathrm{R =} \quad . \tag{2}$$

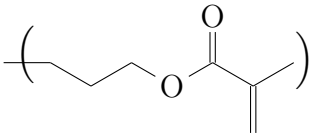

Hydrolyzed monomers then condense into dimers,

$$\mathrm{2\,R{-}Si\,(OH)_3 \rightleftharpoons HO{-}\underset{\mathrm{OH}}{\overset{\mathrm{R}}{\mathrm{Si}}}{-}O{-}\underset{\mathrm{OH}}{\overset{\mathrm{R}}{\mathrm{Si}}}{-}OH + H_2O,} \tag{3}$$

and higher-order branched silsesquioxanes functionalized with propyl methacrylate groups that are insoluble in water and coalesce homogeneously into monodisperse droplets. These nuclei continue to grow in a well-mixed environment until the hydrolyzed monomer is depleted. At this point, the droplets still are fluid but are largely stable against coarsening, because of surface charging.[13] They can be transformed into solid spheres by warming the emulsion to 80 °C and adding a heat-activated free radical initiator to polymerize the methacrylate moieties of the condensed oligomers.

All samples are prepared in identical 12 mL glass vials to produce 5 mL of colloidal dispersion. The vials are sealed to ensure consistent evaporation of ammonia from run to run. Identical stir bars are used for all syntheses to ensure consistent flow properties.

Holographic particle characterization

We perform holographic characterization measurements with a Spheryx xSight, a commercial holographic particle characterization system. The xSight draws a small sample of colloidal suspension through the observation volume of an in-line holographic microscope where it is illuminated with a laser operating at a vacuum wavelength of 532 nm. Light scattered

by a colloidal particle interferes with the rest of the beam in the focal plane of the microscope's objective lens. The objective lens relays this interference pattern to a tube lens that focuses it onto the sensor of a digital video camera. The intensity of the recorded interference pattern is a hologram of the particle that can be analyzed to obtain information about the particle's position and composition. The instrument's analytical software fits each hologram to predictions of the Lorenz-Mie theory of light scattering to measure the associated particle's diameter and refractive index, as well as its three-dimensional position relative to the center of the focal plane.[17] Each particle is recorded and analyzed multiple times during its transit through the observation volume~~to ensure reliable characterization results~~. Time-resolved observations are linked into trajectories using a maximum likelihood algorithm [18], both to map the particle's transit through the sample volume and also to combine multiple independent measurements of that particle's diameter and refractive index for improved accuracy and precision [19]. Typical measurements on micrometer-scale spheres yield a particle's diameter with a precision of 5 nm and its refractive index to within a part

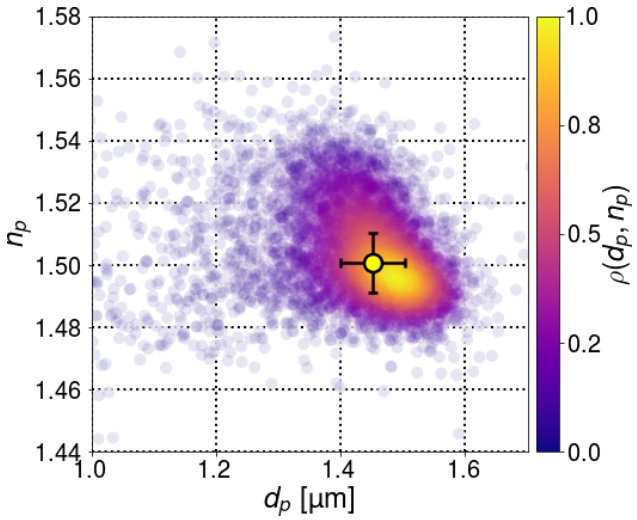

Figure 1: Holographic characterization data for a sample of 1.5 µm-diameter TPM spheres synthesized with 10 µL NH_4OH and 100 µL TPM at a mixing rate of $\Omega = 700\,\mathrm{min}^{-1}$. Each ~~point~~ of the 6935 points represents the diameter, d_p, and refractive index, n_p, of a single sphere and is colored by the relative density of measurements, $\rho(d_p, n_p)$. The cross is centered at the median values of the sample's characteristics and subtends their median-absolute deviations.

per thousand [20,21]. Holographic analysis also yields the particle's in-plane position to within a nanometer and its axial position to within 5 nm [19,20].

Originally demonstrated with dispersions of model colloidal spheres of various compositions [17], holographic particle characterization has been applied successfully to porous particles [22], dimpled spheres [23], and fractal aggregates [24]. It has been used to monitor protein aggregation in biopharmaceuticals [21,25], nanoparticle agglomeration in semiconductor polishing slurries [26] and oil droplet concentration in wastewater [27]. Time-resolved holographic characterization has been used to monitor the growth of colloidal polydimethylsiloxane (PDMS) spheres [28], the response of colloidal sensors to changing environmental conditions [29] and molecular binding to the surface of functionalized beads [19].

xSight measurements are limited to particle concentrations below $10^6\,\mathrm{mL}^{-1}$ to minimize interference of overlapping single-particle holograms. TPM synthesis, however, produces samples with number densities of $10^{10}\,\mathrm{mL}^{-1}$. We therefore dilute each sample by a factor of 10^4 with deionized water before analysis. This should not affect the particles' properties because oligomerized TPM droplets and polymerized spheres are hydrophobic.[13]

We analyze each sample by pipetting 100 µL of the diluted dispersion into an xCell microfluidic sample cell and loading the xCell into the xSight. The xSight draws 3 µL of the fluid through the xCell's 50 µm deep observation volume. A ten-minute measurement provides us with characterization data for a few thousand colloidal spheres per sample. A typical example is presented in Fig. 1. Each point in this plot represents the measured diameter, d_p, and refractive index, n_p, of a single particle. Points are colored by the relative density of observations. This reveals a peak in the distribution at $d_p = 1.5\,\mu\mathrm{m}$ and $n_p = 1.495$. The cross superimposed on the plot indicates the median particle diameter and median refractive index, together with the median absolute deviation in those properties. The spread in measured properties is much larger than the measurement uncertainty provided by xSight, and so represents the polydispersity in the sample's actual properties.

~~Holographic tracking data~~ The measured trajectories of colloidal particles can be used to

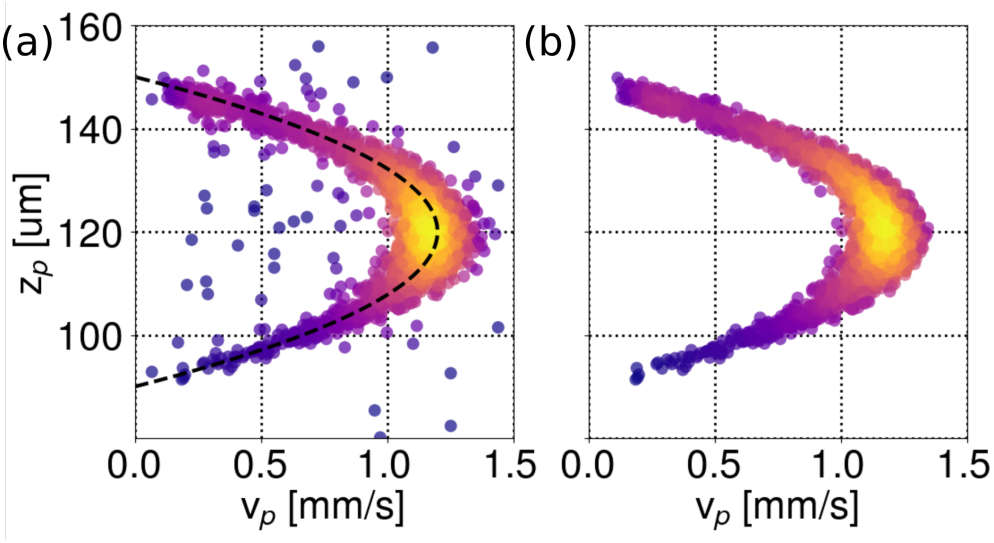

Figure 2: (a) Scatter plot of particle speed, v_p, as a function of height z_p, above the focal plane. Each dot represents tracking data for a single particle and is colored by the density of observations. The dashed blue curve is a fit to a parabola. (b) Filtered results.

monitor the success of a measurement by mapping the Poiseuille flow profile within the xCell microfluidic channel ~~[30]~~ [19,30]. Each point in Fig. 2(a) represents the ~~measured~~ speed, $v_p(z_p)$, for a single particle's transit at its mean axial position, z_p~~, averaged over its trajectory through the observation volume~~. The width of the observed distribution of transit speeds is dominated by variations in the pump speed over the 10 min course of the measurement. These variations do not affect the precision or accuracy of characterization measurements because the flow speed is always low enough to avoid artifacts due to motion blurring [19,31]. The solid curve in Fig. 2(b) is a fit to a ~~parabola~~the expected parabolic flow profile. Extrapolating this fit to ~~$v(z) = 0$~~ $v(z) = 0$ yields estimates for the axial positions of the channel's walls, assuming no-slip boundary conditions. The measured 51 µm range is consistent with the xCell's nominal channel depth. Because the particle's axial position is measured relative to the microscope's focal plane, ~~this result~~ the measured range of z_p can be used to confirm that the xCell is seated properly within the xSight during measurement.

Most observations fall neatly onto the parabolic profile. Some, however, deviate markedly, presumably because of tracking errors ~~due to overlapping holograms. The associated characterization data also~~ that result in particles being misidentified in a sequence of holograms. Tracking

errors are more common in holograms containing multiple particles, particularly when faster-moving particles near the midplane of the channel overtake slower-moving particles near the walls. Characterization data obtained from such faulty tracks are likely to ~~be unreliable~~combine results from different particles rather than reflecting the properties of just one. We therefore reject any features that deviate from the parabolic profile by more than one median absolute deviation, as depicted in Fig. 2(b). In this case, 72 out of 6807 trajectories were cut. The remaining results are used to characterize the sample, and are presented in Fig. 1.

Orthogonal validation methods

Holographic particle characterization is a comparatively new technique and is not yet widely adopted. We therefore validate results from holographic particle characterization with orthogonal measurement techniques. Specifically, we use scanning electron microscopy to provide baseline estimates for the particles' diameters and Abbe refractometry to measure their refractive indexes.

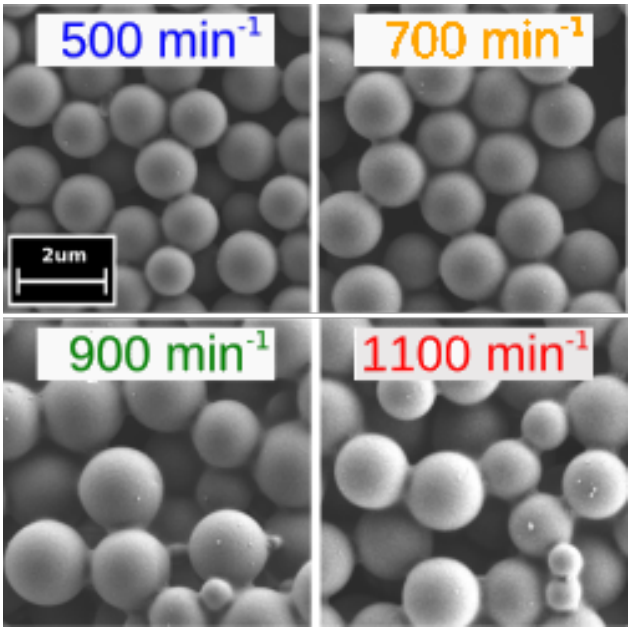

Figure 3: SEM images of polymerized TPM spheres prepared at four different stirring rates.

Each sample of polymerized spheres was imaged with a field emission scanning electron

microscope (MERLIN SEM, Carl Zeiss). Typical images are presented in Fig. 3. SEM images provide a visual check of the spheres' surface texture and can be used to estimate their mean diameter and polydispersity. While a well calibrated scanning electron microscope provides 1 to 10 nm spatial resolution, sample preparation, particularly exposure to vacuum and sputter coating, can shrink or even swell the sample.[9,32] TPM emulsion droplets are fluid and so are not amenable to SEM analysis.

The diameter of an individual sphere is obtained using ImageJ by drawing a tight-fitting oval around its image; the average of each oval's minor and major axes provides an estimate for the associated sphere's diameter [33,34]. The distribution of sphere diameters is estimated by analyzing 50 spheres' images for each sample.

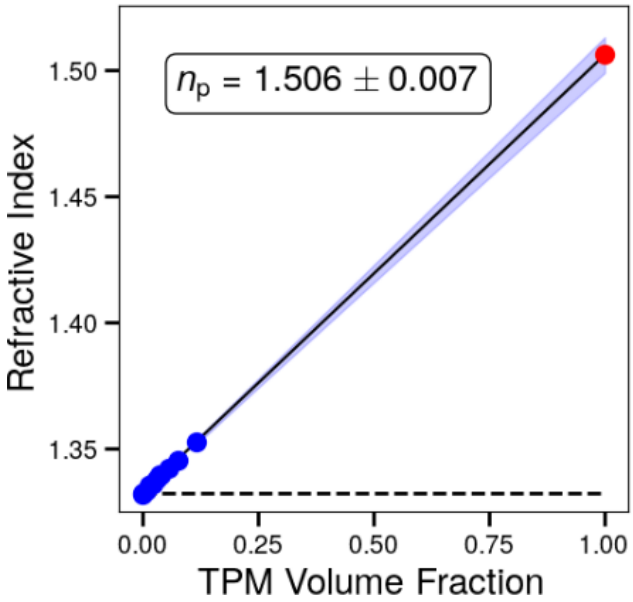

Figure 4: Estimating n_p through refractometry. Discrete (blue) points reflect the refractive index, $n(\phi)$, of 12 suspensions as a function of volume fraction, ϕ. Linear extrapolation to $\phi = 1$ yields an estimate for the refractive index of the dispersed phase, n_p, represented as a red dot. The (blue) shaded region represents the 95 % prediction interval for the extrapolation. The lower dashed line represents the refractive index of water at 532 nm.

We estimate the refractive index of the TPM particles by suspending them in water and measuring the mean refractive index of the suspensions, $n(\phi)$, as a function of the particles' volume fraction, ϕ. Linearly extrapolating to $\phi = 1$ yields an estimate for the spheres' refractive index, n_p, in their native medium at room temperature 21.5 °C.[35] Figure 4 shows

an application of this technique to two similarly prepared samples of TPM spheres. ~~Each sample was~~ The initial number density of particles in each sample is obtained with the xSight by counting the particles in 2 µL of fluid. This approach yields particle concentrations with an accuracy of 10 % in the range from 10^3 particles/mL to 10^7 particles/mL [21]. Each sample is diluted to 5 different volume fractions to provide a total of 12 different suspensions, including the two stock samples. The refractive index of each suspension was measured with an Abbe refractometer at room temperature 21.5 °C. Linear extrapolation yields $n_p = 1.506 \pm 0.007$ with 95 % confidence. This range includes uncertainty in the samples volume fractions as well as any differences between the two samples.

This method is complementary to the approach used by van der Wel, *et al.*, who index matched their particles to a solution of pyridine ($n = 1.509$) and 2-ethylhexyl 4-methoxycinnamate ($n = 1.545$) and identified the refractive index of the particles with that of the best index matching solution.[13] They report the refractive index to be between 1.512 and 1.513, presumably at a wavelength of 589 nm.

Optimization strategies

The immediate goal of this study is to design a synthesis protocol that reproducibly yields TPM spheres with a selected size and the smallest degree of polydispersity in size. Factors governing size selection include ammonia concentration, emulsion stoichiometry, and mixing conditions. These factors determine the nucleation rate of oligomer droplets, the rate and duration of growth, and the homogeneity of these processes, respectively.

The choice of free-radical initiator should not affect the size distribution of the oligomer droplets, but may influence the course of polymerization, and thus the density and size of the final spheres. Oil-soluble initiators might be expected to polymerize the spheres uniformly thereby shrinking the spheres as the material becomes more dense. Water-soluble initiators, by contrast, might polymerize the spheres from the surface inward, perhaps inhibiting shrinkage and producing a larger and less dense product.

To guide protocol design, we first monitor the effect of mixing conditions on size selection during droplet formation. Using holographic characterization data to monitor polymerization speeds the optimization process by identifying when processing has run to completion. We then use the optimal mixing conditions for a binary search through parameter space of ammonia concentration and TPM stoichiometry. Finally, we assess the influence of initiator choice on particle properties.

Results and Discussion

Each holographic particle characterization measurement requires roughly 15 min including sample preparation and yields a comprehensive view of the joint distribution of the sizes and refractive indexes of the particle in the sample. Orthogonal techniques yield information about the size distribution or about the refractive index distribution separately. We therefore use these techniques to validate size data and composition data independently.

Effect of stirring rate on particle size

~~Probability distribution function (PDF) for sphere diameters as measured by holographic particle characterization (HPC) and by SEM for samples that were stirred at 500 (blue), 700 (yellow), 900 (green), and 1100 min^{-1} (red). HPC results are projections of joint distributions such as the example in Fig. 1 and each summarize several thousand single-particle measurements. Histograms of SEM results were compiled from images of dried samples such as the examples in Fig. 3.~~

Stirring the sample while the oligomers condense into droplets promotes homogeneous nucleation by uniformly dispersing the hydrolyzed monomer and droplet nuclei, thereby ensuring that all droplets grow under comparable conditions. Beyond simply mixing the sample, however, stirring creates shear forces[36] that can alter droplets' size distribution.[37,38] The overall effect of stir rate on the resulting particle size is best assessed experimentally.

Figure 5 summarizes how stirring rate influences the size of TPM spheres for a given set of synthesis conditions. The four emulsions represented in this plot were produced in identical cylindrical vials with identical stir bars. Each vial was charged with 15 µL of 29 % ammonia (29.3 % NH_3(aq) by HCl titration) using an Eppendorf Research plus pipette, followed by 200 µL of TPM monomer and was immediately brought up to 5 mL with DI water. These conditions yield pH = 11.0 and [TPM] = 0.16 M. The four samples were stirred for 2 h using magnetic stir plates set at 500, 700, 900, and 1100 min^{-1}. The resulting droplets were polymerized by adding an excess (1 mg) of AIBN as a radical initiator and heating the sample to 80 °C for 2 h. These samples then were analyzed by both HPC and SEM.

The mixing conditions are set by the geometry of the vial, the shape of the stir rod, and the stir rate. The 12 mL cylindrical vials have an inner diameter of 16 mm and a height of 60 mm. Each 5 mL sample filled approximately one third of the cylinder's volume. Each pill-shaped magnetic stir rod has a long axis length of 12 mm and short axis length of 7 mm. The dimensionless impeller Reynolds number distinguishes turbulent and laminar flows and is given as

$$N_{Re} = \frac{\Omega d^2 \rho}{\mu}, \tag{4}$$

where Ω is the rotation speed in rotations per second, d is the impeller diameter, and ρ and μ refer to the density and dynamic viscosity of water, respectively. Therefore the impeller Reynolds number varies from 3200 at a stir rate of 500 min^{-1} to 7000 at 1100 min^{-1}. This means that the tangential flow is turbulent over the entire range.[36] The meniscus of the driven vortex ranges in depth from 5 mm at 500 min^{-1} to 20 mm at 1100 min^{-1}, and does not reach the stir bar until 2000 min^{-1}. Flow conditions therefore should be comparable over the entire range of stirring rates considered.

The results in Fig. 5 reveal that the smallest mean particle size is obtained at the lowest stirring speeds. This surprising observation runs counter to the usual trend[37,38] in emulsion polymerization[39] and suspension polymerization.[40] Increasing stirring speed also increases the particles' polydispersity, particularly increasing the proportion of undersized particles.

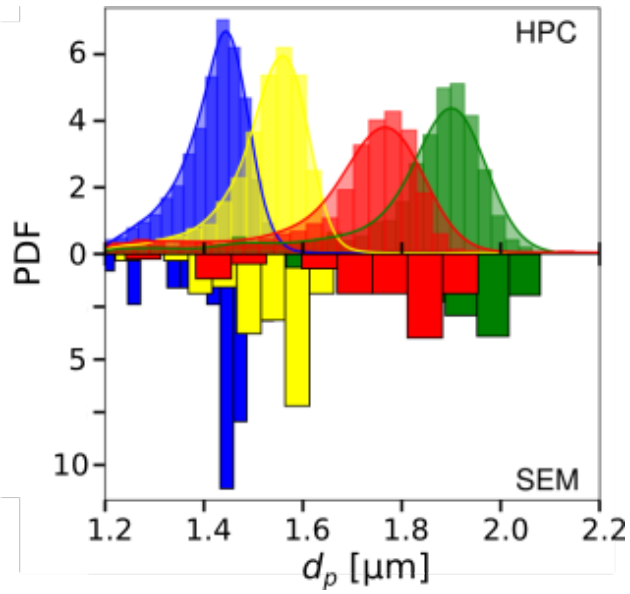

Figure 5: Probability distribution function (PDF) for sphere diameters as measured by holographic particle characterization (HPC) and by SEM for samples that were stirred at 500 (blue), 700 (yellow), 900 (green), and 1100 min^{-1} (red). HPC results are projections of joint distributions such as the example in Fig. 1 and each summarize several thousand single-particle measurements. Histograms of SEM results were compiled from images of dried samples such as the examples in Fig. 3.

It is possible that increasing shear rate favors collision-induced droplet coalescence in this system [41]. The samples' ~~mean~~ median diameters, $\langle d_\mathrm{p} \rangle$, are reported in Table 1 together with their standard deviations, σ_{d_p}.

Table 1: Median size and standard deviation of TPM spheres measured by SEM analysis and holographically for each of the four stir rates.

Ω [min^{-1}]	500	700	900	1100
$\langle d_p \rangle_{\mathrm{SEM}}$ [µm]	1.45	1.56	1.92	1.75
$\sigma_{d_p,\mathrm{SEM}}$ [µm]	0.12	0.13	0.28	0.32
$\langle d_p \rangle_{\mathrm{HPC}}$ [µm]	1.43	1.54	1.88	1.73
$\sigma_{d_p,\mathrm{HPC}}$ [µm]	0.04	0.05	0.06	0.08

Size distributions obtained holographically are consistent with results of SEM analysis on the same samples, including the images in Fig. 3. ~~The mean sphere diameter is estimated by analyzing 50 spheres' images using ImageJ [34]. The diameter of an individual sphere is obtained drawing a tight-fitting oval around its image; the average of each oval's minor~~

~~and major axes provides an estimate for the associated sphere's diameter. The resulting histograms of particle diameters~~ These results also are plotted in Fig. 5 and reported in Table 1. For all samples, the median particle diameter obtained holographically agrees with the median SEM result to within 40 nm, which is smaller than the sample standard deviation. This agreement supports our use of HPC for rapid sample characterization.

Based on the outcome of this survey, we synthesize the remainder of the particles in this study at a stirring rate of $700\,\mathrm{min}^{-1}$, which yields particles with the smallest relative polydispersity.

~~Median size and standard deviation of TPM spheres measured by SEM analysis and holographically for each of the four stir rates.~~ ~~Ω [min^{-1}] 500 700900 1100 $\langle d_p \rangle_{\mathrm{SEM}}$ [µm] 1.45 1.56 1.92 1.75 $\sigma_{d_p,\mathrm{SEM}}$ [µm] 0.12 0.13 0.28 0.32 $\langle d_p \rangle_{\mathrm{HPC}}$ [µm] 1.43 1.54 1.88 1.73 $\sigma_{d_p,\mathrm{HPC}}$ [µm] 0.04 0.05 0.06 0.08~~

Although unpolymerized droplets are not amenable to SEM analysis, they can be by analyzed holographically. Figure 6 presents the median size and refractive index of TPM emulsion droplets prepared at the four stirring rates, both before and after polymerization. Overall the influence of polymerization on median droplet diameter is consistent with the 2 % reduction in size reported by van der Wel, *et al.* based on dynamic light scattering.[13]

Effect of stirring rate on refractive index

Figure 6 summarizes holographic characterization results for the influence of stirring rate on the properties of TPM emulsions and their associated polymerized dispersion. Each dot represents the median size and refractive index for the associated sample. Error bars represent the median absolute deviations of those properties.

Whereas stirring has a substantial influence on droplet size, its effect on refractive index is slight at most. This is reasonable because the refractive index reflects the composition of the condensed phase, which should not be substantially influenced by local flow conditions. The polymerized spheres have an average refractive index of $n_p = 1.501 \pm 0.009$, which is

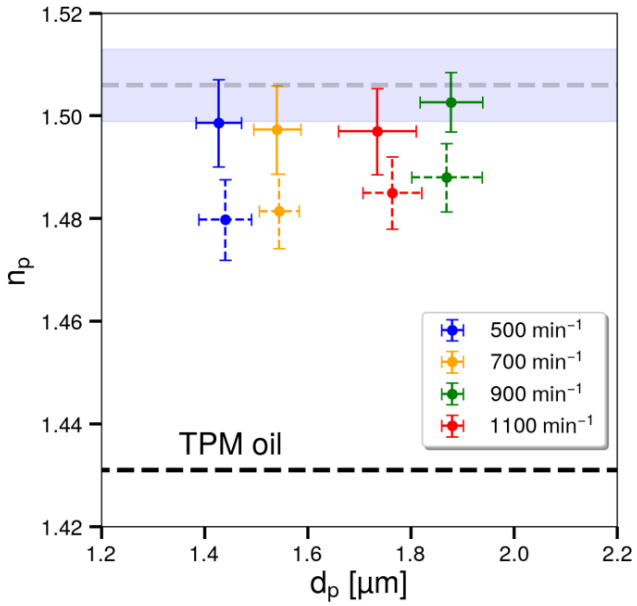

Figure 6: Holographic characterization of emulsion droplets (dashed lines) and polymerized spheres (solid lines) stirred at 4 different rates. Filled circles represents the median diameter and refractive index for one sample. Error bars represent one median absolute deviation from the median. The dashed black line represents the refractive index of monomeric TPM oil. The dashed gray line represents the refractive index for polymerized TPM spheres obtained with conventional refractometry, including the 95 % prediction interval.

consistent with conventional refractometry. The unpolymerized emulsion droplets have a systematically lower refractive index. Polymerization changes the chemical makeup of the droplet and generally increases the density and so might reasonably account for the observed change in refractive index.

The refractive indexes of TPM droplets and polymerized spheres both substantially exceed that of bulk TPM oil, which is indicated by a dashed line in Fig. 6. Hydrolysis and oligomerization account for a refractive index shift of roughly 0.05 and polymerization accounts for the remaining increase of 0.02.

Monitoring polymerization

The small but clearly resolved change in droplet size and refractive index can be used to monitor the progress of polymerization. This is useful both for ensuring that polymerization has run to completion before analysis, and also for minimizing the time required for

combinatorial studies of processing choices.

Figure 7 illustrates how holographic characterization can be used to monitor droplet polymerization. This sample consists of an emulsion of TPM droplets and the initiator AIBN. The suspension is continuously stirred at 1100 min^{-1} and is thermally coupled to a heat bath set at 80 °C. Starting when the initiator is added, we draw 1 µl of the suspension after 5, 10, 15, 20, 40, 60 min. Each aliquot is added immediately to 10 mL of room temperature deionized water to arrest polymerization through thermal quenching. The diluted sample then is transferred to the xSight for analysis.

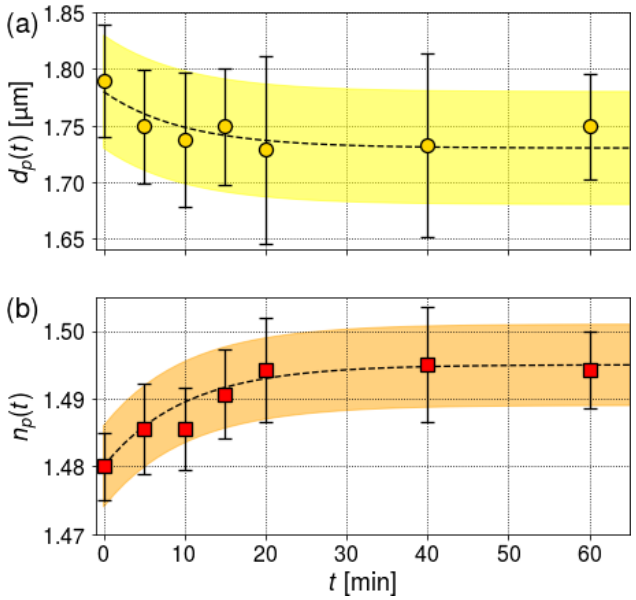

Figure 7: Particle properties after heat bath exposure times of 5, 10, 15, 20, 40, and 60 min. (a) The average size and (b) refractive index of particles as a function of heat bath exposure time. Error bars indicate a single median absolute deviation of the associated property.

The median diameter of the TPM droplets plotted in Fig. 7(a) decreases by 2 % on average during polymerization. Although this is well within the measured polydispersity of each sample, it is consistent with the 7 % reduction in volume reported in Ref. [13]. The change in size is correlated with a simultaneous increase in the refractive index from 1.485 to 1.495 that is plotted in Fig. 7(b).

Dashed curves in Fig. 7 are exponentials with a 10 min characteristic time that are superimposed on the data as a guide to the eye. Changes in dispersion properties have largely run

their course in 20 min. All four initiators are active for this period with half-lives at 80 °C of 1.8 h (APS[42]), 2 h (KPS[43]), 6 h (AIBN) and 30 h (ACHN). The results in Fig. 7 therefore suggest that heating for more than half an hour will not substantially alter these particles' properties. Because holographic characterization can be performed in a matter of minutes, this information can be used to minimize heating time and thus energy cost in emulsion polymerization. We use this information to ensure that all syntheses have run to completion in assessing the role of emulsion stoichiometry and initiator selection on particle properties.

Effect of emulsion stoichiometry and initiator solubility

The amount of hydrolyzed TPM oil in solution influences both the number of droplets that nucleate and the size to which they grow. The outcome also depends on the pH of the solution, influences the rate of oligomerization and should influence the droplets' polydispersity. To identify conditions that minimize polydispersity, we prepare four batches of droplets corresponding to binary choices in the concentrations of TPM oil and ammonia. In each case, TPM oil is injected into an ammonia solution with stirring. Two samples are prepared with 81 mmol L^{-1} TPM and another two with 122 mmol L^{-1}. In each case, one of the samples is prepared with 31.8 mmol L^{-1} of ammonia, and the other with 61.5 mmol L^{-1}, which correspond to pH 10.87 and pH 11.02, respectively.

How the droplets polymerize may depend on the solubility of the initiator. Water-soluble initiators, for example, are believed to polymerize particles from the surface inward, leading to inhomogeneous solidification.[14] Such particles might differ appreciably from those polymerized with oil-soluble initiators that presumably would be more homogeneously solidified. To investigate this effect, each of the four emulsions is polymerized with four different initiators: two oil-soluble initiators, AIBN and ACHN, and two water-soluble initiators, potassium persulfate and ammonium persulfate. This yields a total of 16 samples.

Both types of initiators are at least slightly soluble in both phases. The oil-soluble initiators therefore reach the droplets through the aqueous phase. The water-soluble initiations,

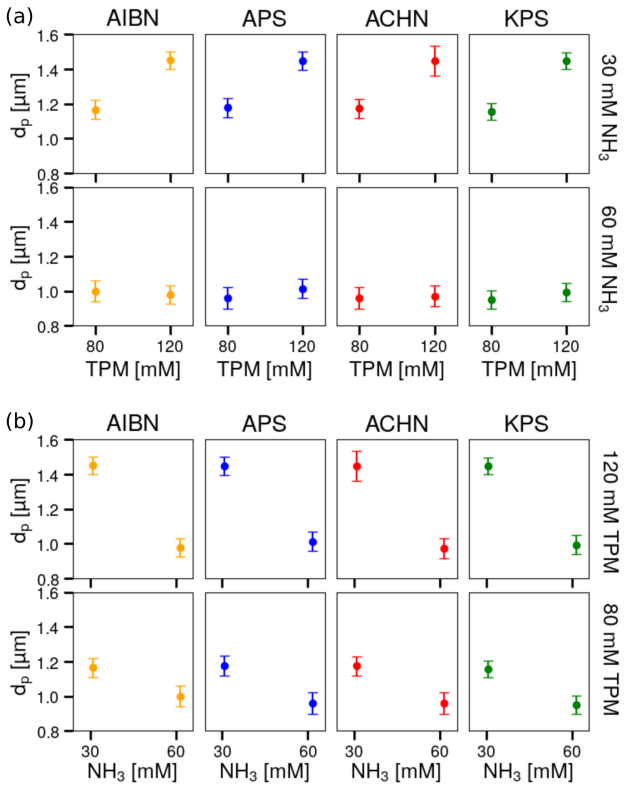

Figure 8: (a) Median diameter as a function of TPM content at fixed ammonia concentration. (b) Median diameter as a function of ammonia concentration at fixed TPM content.

moreover, can permeate the spheres.

Figure 8 presents characterization data from all 16 data sets plotted to highlight different binary choices. Each point represents the median properties of one of the samples and is amassed from several thousand individual holographic characterization measurements. Figure 8(a) emphasizes the influence of TPM concentration on the polymerized particle diameter for fixed concentration of ammonia and choice of initiator. Increasing TPM content increases particle diameter at low concentration of ammonia, but has less influence at higher concentration of ammonia. Increasing the concentration of ammonia therefore improves reproducibility by reducing sensitivity to variations in TPM concentration.

Figure 8(b) shows the complementary projection of the data that emphasizes the influence of ammonia concentration. All eight assays convey the same message: increasing ammonia concentration decreases the average particle diameter. Increased ammonia increases surface

charge, which promotes nucleated particle stability.[13] This, in turn, favors higher particle number density and smaller particle size for a given amount of TPM monomer. Increasing the number and stability of nuclei has the additional effect of improving predictability of the particle radius by reducing sensitivity to the amount of TPM.

Choice of initiator has no appreciable influence on the finished particles' average diameter. Size selection is predominantly determined by nucleation and growth of oligomerized TPM droplets. The concentration of ammonia increases the pH and therefore increases the rate at which TPM hydrolizes and oligomerizes. Faster nucleation presumably yields more droplets and reduces the average particle size. At low concentrations of ammonia, oligomerization proceeds more slowly and ~~and~~ yields fewer larger droplets.

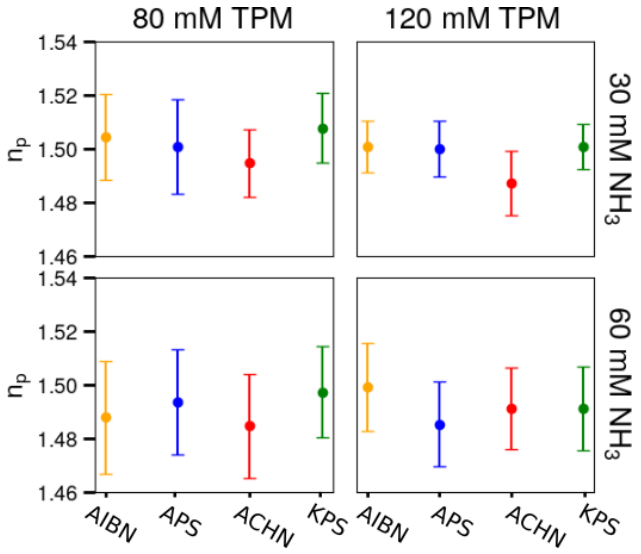

Figure 9: Median refractive index reported for each radical initiator at fixed concentration of TPM.

The choice of initiator also has no substantial influence on the particles' refractive indexes, as shown in Fig. 9. This is surprising because larger TPM droplets are known to form dimples when polymerized with the water-soluble initiators.[14] Dimpling is believed to result from surface hardening followed by ejection of low-molecular-weight oligomers.[14] Smaller TPM spheres polymerized with these initiators do not form dimples and so might be expected to have nonuniform densities with possible signatures in the measured refractive index. In fact,

no significant differences are observed.

Summary and Conclusions

We have demonstrated some of the ways in which holographic particle characterization can be used to guide the development of synthesis protocols for colloidal particles. Our specific study of monodisperse TPM spheres examines the influence of particular protocol choices on the size and refractive index of the resulting polymerized spheres. Specifically, we investigate the roles of stirring rate, incubation time, stoichiometry, and choice of free radical initiator.

Increasing stirring rate is found to increase particle size at the cost of increasing polydispersity. Increasing pH through the concentration of ammonia decreases particle size and enhances reproducibility.

Unlike orthogonal techniques, holographic characterization requires minimal sample preparation and provides results in minutes, and so can be used for feedback at all stages in the synthesis. Periodically sampling the reaction vessel, for example, is useful for determining when droplet growth has run to completion.

These results demonstrate that holographic characterization can be a valuable addition to the arsenal of techniques used to design and control colloidal synthesis protocols.

Acknowledgement

This work was supported primarily by the MRSEC program of the National Science Foundation through Award Number DMR-1420073. Additional support was provided by the SBIR program of the National Science Foundation through Award Number IPP-1519057, and in part by NASA under grant award NNX13AR67G. The Spheryx xSight holographic characterization instrument used in this study was acquired by the NYU MRSEC as a shared instrument. The Zeiss scanning electron microscope used in this study was acquired under NSF Award Number DMR-0923251 and is maintained as a shared facility by the NYU

MRSEC.

makeother‘{=1 ‘}=2 @aux@ifundefined

Backus, R. C.; Williams, R. C. Small spherical particles of exceptionally uniform size. *J. Appl. Phys.* **1949**, *20*, 224–225Gerould, C. H. Comments on the use of latex spheres as size standards in electron microscopy. *J. Appl. Phys.* **1950**, *21*, 183–184Vanderhoff, J.; Vitkuske, J.; Bradford, E.; Alfrey Jr, T. Some factors involved in the preparation of uniform particle size latexes. *J. Polym. Sci.* **1956**, *20*, 225–234Stöber, W.; Fink, A.; Bohn, E. Controlled growth of monodisperse silica spheres in the micron size range. *J. Colloid Interf. Sci.* **1968**, *26*, 62–69Kotera, A.; Furusawa, K.; Kudō, K. Colloid chemical studies of polystyrene latices polymerized without any surface-active agents. I.Method for preparing monodisperse latices and their characterization. *Kolloid Z. Z. Polym.* **1970**, *240*, 837–842Deželić, N.; Peters, J. J.; Deželić, Gj. Preparation of monodisperse polystyrene latices. *Kolloid Z. Z. Polym.* **1970**, *242*, 1142–1150Goodwin, J.; Hearn, J.; Ho, C.; Ottewill, R. Studies on the preparation and characterisation of monodisperse polystyrene latices. III.Preparation without added surface active agents. *Colloid Polym. Sci.* **1974**, *252*, 464–471Antl, L.; Goodwin, J.; Hill, R.; Ottewill, R. H.; Owens, S.; Papworth, S.; Waters, J. The preparation of poly (methyl methacrylate) latices in non-aqueous media. *Colloids Surf.* **1986**, *17*, 67–78Yamada, Y.; Miyamoto, K.; Koizumi, A. Size determination of latex particles by electron microscopy. *Aerosol Sci. Techn.* **1985**, *4*, 227–232Giesche, H. Mercury porosimetry: a general (practical) overview. *Part. Part. Syst. Character.* **2006**, *23*, 9–19Rouquerol, J.; Avnir, D.; Fairbridge, C.; Everett, D.; Haynes, J.; Pernicone, N.; Ramsay, J.; Sing, K.; Unger, K. Recommendations for the characterization of porous solids (Technical Report). *Pure Appl. Chem.* **1994**, *66*, 1739–1758Chou, A.; Kerker, M. The refractive index of colloidal sols. *J. Phys. Chem.* **1956**, *60*, 562–564van der Wel, C.; Bhan, R. K.; Verweij, R. W.; Frijters, H. C.; Gong, Z.; Hollingsworth, A. D.; Sacanna, S.; Kraft, D. J. Preparation of colloidal organosilica spheres through spontaneous emulsification. *Langmuir* **2017**, *33*, 8174–8180Sacanna, S.; Irvine, W. T. M.; Rossi, L.; Pine, D. J. Lock and key colloids through

polymerization-induced buckling of monodisperse silicon oil droplets. *Soft Matter* **2011**, *7*, 1631–1634Liu, Y.; Edmond, K. V.; Curran, A.; Bryant, C.; Peng, B.; Aarts, D. G. A. L.; Sacanna, S.; Dullens, R. P. A. Coreshell particles for simultaneous 3D imaging and optical tweezing in dense colloidal materials. *Adv. Mater.* **2016**, *28*, 8001–8006van der Wel, C.; van de Stolpe, G. L.; Verweij, R. W.; Kraft, D. J. Micrometer-sized TPM emulsion droplets with surface-mobile binding groups. *J. Phys. Cond. Matt.* **2018**, *30*, 094005Lee, S.-H.; Roichman, Y.; Yi, G.-R.; Kim, S.-H.; Yang, S.-M.; van Blaaderen, A.; van Oostrum, P.; Grier, D. G. Characterizing and tracking single colloidal particles with video holographic microscopy. *Opt. Express* **2007**, *15*, 18275–18282Cheong, F. C.; Krishnatreya, B. J.; Grier, D. G. Strategies for three-dimensional particle tracking with holographic video microscopy. *Opt. Express* **2010**, *18*, 13563–13573Jung, K.; Park, B.; Song, W.; O, B.-H.; Eom, T. Measurement of 100-nm polystyrene sphere by transmission electron microscope. *Powder Tech.* **2002**, *126*, 255–265Alexander, K.; Killey, A.; Meeten, G.; Senior, M. Refractive index of concentrated colloidal dispersions. *J. Chem. Soc. Faraday Trans. 2* **1981**, *77*, 361–372Halász, G.; Gyüre, B.; Jánosi, I. M.; Szabó, K. G.; Tél, T. Vortex flow generated by a magnetic stirrer. *Am. J. Phys.* **2007**, *75*, 1092–1098Oles, V. Shear-induced aggregation and breakup of polystyrene latex particles. *J. Colloid Interface Sci.* **1992**, *154*, 351–358Eggersdorfer, M.; Kadau, D.; Herrmann, H. J.; Pratsinis, S. E. Fragmentation and restructuring of soft-agglomerates under shear. *J. Colloid Interface Sci.* **2010**, *342*, 261–268Chern, C. Emulsion polymerization mechanisms and kinetics. *Prog. Polym. Sci.* **2006**, *31*, 443–486Arshady, R. Suspension, emulsion, and dispersion polymerization: A methodological survey. *Colloid Polym. Sci.* **1992**, *270*, 717–732Mazzoli, A.; Favoni, O. Particle size, size distribution and morphological evaluation of airborne dust particles of diverse woods by Scanning Electron Microscopy and image processing program. *Powder Tech.* **2012**, *225*, 65–71Borisov, I.; Luksha, R.; Rashidova, S. Kinetic features of ammonium persulfate decomposition in aqueous medium. *Russian Chem. Bull.* **2015**, *64*, 2512–2513Beylerian, N. M.; Vardanyan, L. R.; Harutyunyan, R. S.; Vardanyan, R. L. Kinetics and mechanism of potassium persulfate decomposition in aqueous

solutions studied by a gasometric method. *Macromol. Chem. Phys.* **2002**, *203*, 212–218

References

(1) Backus, R. C.; Williams, R. C. Small spherical particles of exceptionally uniform size. *J. Appl. Phys.* **1949**, *20*, 224–225.

(2) Gerould, C. H. Comments on the use of latex spheres as size standards in electron microscopy. *J. Appl. Phys.* **1950**, *21*, 183–184.

(3) Vanderhoff, J.; Vitkuske, J.; Bradford, E.; Alfrey Jr, T. Some factors involved in the preparation of uniform particle size latexes. *J. Polym. Sci.* **1956**, *20*, 225–234.

(4) Stöber, W.; Fink, A.; Bohn, E. Controlled growth of monodisperse silica spheres in the micron size range. *J. Colloid Interf. Sci.* **1968**, *26*, 62–69.

(5) Kotera, A.; Furusawa, K.; Kudō, K. Colloid chemical studies of polystyrene latices polymerized without any surface-active agents. I. Method for preparing monodisperse latices and their characterization. *Kolloid Z. Z. Polym.* **1970**, *240*, 837–842.

(6) Deželić, N.; Peters, J. J.; Deželić, Gj. Preparation of monodisperse polystyrene latices. *Kolloid Z. Z. Polym.* **1970**, *242*, 1142–1150.

(7) Goodwin, J.; Hearn, J.; Ho, C.; Ottewill, R. Studies on the preparation and characterisation of monodisperse polystyrene latices. III. Preparation without added surface active agents. *Colloid Polym. Sci.* **1974**, *252*, 464–471.

(8) Antl, L.; Goodwin, J.; Hill, R.; Ottewill, R. H.; Owens, S.; Papworth, S.; Waters, J. The preparation of poly (methyl methacrylate) latices in non-aqueous media. *Colloids Surf.* **1986**, *17*, 67–78.

(9) Yamada, Y.; Miyamoto, K.; Koizumi, A. Size determination of latex particles by electron microscopy. *Aerosol Sci. Techn.* **1985**, *4*, 227–232.

(10) Giesche, H. Mercury porosimetry: a general (practical) overview. *Part. Part. Syst. Character.* **2006**, *23*, 9–19.

(11) Rouquerol, J.; Avnir, D.; Fairbridge, C.; Everett, D.; Haynes, J.; Pernicone, N.; Ramsay, J.; Sing, K.; Unger, K. Recommendations for the characterization of porous solids (Technical Report). *Pure Appl. Chem.* **1994**, *66*, 1739–1758.

(12) Chou, A.; Kerker, M. The refractive index of colloidal sols. *J. Phys. Chem.* **1956**, *60*, 562–564.

(13) van der Wel, C.; Bhan, R. K.; Verweij, R. W.; Frijters, H. C.; Gong, Z.; Hollingsworth, A. D.; Sacanna, S.; Kraft, D. J. Preparation of colloidal organosilica spheres through spontaneous emulsification. *Langmuir* **2017**, *33*, 8174–8180.

(14) Sacanna, S.; Irvine, W. T. M.; Rossi, L.; Pine, D. J. Lock and key colloids through polymerization-induced buckling of monodisperse silicon oil droplets. *Soft Matter* **2011**, *7*, 1631–1634.

(15) Liu, Y.; Edmond, K. V.; Curran, A.; Bryant, C.; Peng, B.; Aarts, D. G. A. L.; Sacanna, S.; Dullens, R. P. A. Coreshell particles for simultaneous 3D imaging and optical tweezing in dense colloidal materials. *Adv. Mater.* **2016**, *28*, 8001–8006.

(16) van der Wel, C.; van de Stolpe, G. L.; Verweij, R. W.; Kraft, D. J. Micrometer-sized TPM emulsion droplets with surface-mobile binding groups. *J. Phys. Cond. Matt. 30*, 094005.

(17) Lee, S.-H.; Roichman, Y.; Yi, G.-R.; Kim, S.-H.; Yang, S.-M.; van Blaaderen, A.; van Oostrum, P.; Grier, D. G. Characterizing and tracking single colloidal particles with video holographic microscopy. *Opt. Express* **2007**, *15*, 18275–18282.

(18) Crocker, J. C.; Grier, D. G. Methods of digital video microscopy for colloidal studies. *J. Colloid Interface Sci.* **1996**, *179*, 298–310.

(19) Cheong, F. C.; Dreyfus, B. S. R.; Amato-Grill, J.; Xiao, K.; Dixon, L.; Grier, D. G. Flow visualization and flow cytometry with holographic video microscopy. *Opt. Express* **2009**, *17*, 13071–13079.

(20) Krishnatreya, B. J.; Colen-Landy, A.; Hasebe, P.; Bell, B. A.; Jones, J. R.; Sunda-Meya, A.; Grier, D. G. Measuring Boltzmann's constant through holographic video microscopy of a single sphere. *Am. J. Phys.* **2014**, *82*, 23–31.

(21) Wang, C.; Zhong, X.; Ruffner, D. B.; Stutt, A.; Philips, L. A.; Ward, M. D.; Grier, D. G. Holographic characterization of protein aggregates. *J. Pharm. Sci.* **2016**, *105*, 1074–1085.

(22) Cheong, F. C.; Xiao, K.; Pine, D. J.; Grier, D. G. Holographic characterization of individual colloidal spheres' porosities. *Soft Matter* **2011**, *7*, 6816–6819.

(23) Hannel, M.; Middleton, C.; Grier, D. G. Holographic characterization of imperfect colloidal spheres. *Applied Physics Letters* **2015**, *107*, 141905.

(24) Wang, C.; Cheong, F. C.; Ruffner, D. B.; Zhong, X.; Ward, M. D.; Grier, D. G. Holographic characterization of colloidal fractal aggregates. *Soft Matter* **2016**, *12*, 8774–8780.

(25) Kasimbeg, P. N.; Cheong, F. C.; Ruffner, D. B.; Blusewicz, J. M.; Philips, L. A. Holographic Characterization of Protein Aggregates in the Presence of Silicone Oil and Surfactants. *J. Pharm. Sci.* **2019**, *108*, 155–161.

(26) Cheong, F. C.; Kasimbeg, P.; Ruffner, D. B.; Hlaing, E. H.; Blusewicz, J. M.; Philips, L. A.; Grier, D. G. Holographic characterization of colloidal particles in turbid media. *Appl. Phys. Lett.* **2017**, *111*, 153702.

(27) Philips, L. A.; Ruffner, D. B.; Cheong, F. C.; Blusewicz, J. M.; Kasimbeg, P.; Waisi, B.; McCutcheon, J. R.; Grier, D. G. Holographic characterization of contaminants in water:

Differentiation of suspended particles in heterogeneous dispersions. *Water Research* **2017**, *122*, 431–439.

(28) Wang, C.; Shpaisman, H.; Hollingsworth, A. D.; Grier, D. G. Celebrating Soft Matter's 10th anniversary: Monitoring colloidal growth with holographic microscopy. *Soft Matter* **2015**, *11*, 1062–1066.

(29) Wang, C.; Moyses, H. W.; Grier, D. G. Stimulus-responsive colloidal sensors with fast holographic readout. *Appl. Phys. Lett.* **2015**, *107*, 051903.

(30) Cheong, F. C.; Krishnatreya, B. J.; Grier, D. G. Strategies for three-dimensional particle tracking with holographic video microscopy. *Opt. Express* **2010**, *18*, 13563–13573.

(31) Dixon, L.; Cheong, F. C.; Grier, D. G. Holographic particle-streak velocimetry. *Opt. Express* **2011**, *19*, 4393–4398.

(32) Jung, K.; Park, B.; Song, W.; O, B.-H.; Eom, T. Measurement of 100-nm polystyrene sphere by transmission electron microscope. *Powder Tech.* **2002**, *126*, 255–265.

(33) Klein, T.; Buhr, E.; Johnsen, K.; Frase, C. Traceable measurement of nanoparticle size using a scanning electron microscope in transmission mode (TSEM). *Meas. Sci. Technol.* **2011**, *22*, 094002.

(34) Mazzoli, A.; Favoni, O. Particle size, size distribution and morphological evaluation of airborne dust particles of diverse woods by Scanning Electron Microscopy and image processing program. *Powder Tech.* **2012**, *225*, 65–71.

(35) Alexander, K.; Killey, A.; Meeten, G.; Senior, M. Refractive index of concentrated colloidal dispersions. *J. Chem. Soc. Faraday Trans. 2* **1981**, *77*, 361–372.

(36) Halász, G.; Gyüre, B.; Jánosi, I. M.; Szabó, K. G.; Tél, T. Vortex flow generated by a magnetic stirrer. *Am. J. Phys.* **2007**, *75*, 1092–1098.

(37) Oles, V. Shear-induced aggregation and breakup of polystyrene latex particles. *J. Colloid Interface Sci.* **1992**, *154*, 351–358.

(38) Eggersdorfer, M.; Kadau, D.; Herrmann, H. J.; Pratsinis, S. E. Fragmentation and restructuring of soft-agglomerates under shear. *J. Colloid Interface Sci.* **2010**, *342*, 261–268.

(39) Chern, C. Emulsion polymerization mechanisms and kinetics. *Prog. Polym. Sci.* **2006**, *31*, 443–486.

(40) Arshady, R. Suspension, emulsion, and dispersion polymerization: A methodological survey. *Colloid Polym. Sci.* **1992**, *270*, 717–732.

(41) Yeung, A.; Moran, K.; Masliyah, J.; Czarnecki, J. Shear-induced coalescence of emulsified oil drops. *J. Colloid Interface Sci.* **2003**, *265*, 439–443.

(42) Borisov, I.; Luksha, R.; Rashidova, S. Kinetic features of ammonium persulfate decomposition in aqueous medium. *Russian Chem. Bull.* **2015**, *64*, 2512–2513.

(43) Beylerian, N. M.; Vardanyan, L. R.; Harutyunyan, R. S.; Vardanyan, R. L. Kinetics and mechanism of potassium persulfate decomposition in aqueous solutions studied by a gasometric method. *Macromol. Chem. Phys.* **2002**, *203*, 212–218.

Graphical TOC Entry